

Non-Hermitian zero-energy pinning of Andreev and Majorana bound states in superconductor-semiconductor systems

Jorge Cayao¹

¹*Department of Physics and Astronomy, Uppsala University, Box 516, S-751 20 Uppsala, Sweden*

(Dated: August 21, 2024)

The emergence of Majorana bound states in finite length superconductor-semiconductor hybrid systems has been predicted to occur in the form of oscillatory energy levels with parity crossings around zero energy. Each zero-energy crossing is expected to produce a quantized zero-bias conductance peak but several studies have reported conductance peaks pinned at zero energy over a range of Zeeman fields, whose origin, however, is not clear. In this work we consider superconducting systems with spin-orbit coupling under a Zeeman field and demonstrate that non-Hermitian effects, due to coupling to ferromagnet leads, induce zero-energy pinning of Majorana and trivial Andreev bound states. We find that this zero-energy pinning effect occurs due to the formation of non-Hermitian spectral degeneracies known as exceptional points, whose emergence can be controlled by the interplay of non-Hermiticity, the applied Zeeman field, and chemical potentials. Moreover, depending on the non-Hermitian spatial profile, we find that non-Hermiticity changes the single point Hermitian topological phase transition into a flattened zero energy line bounded by exceptional points from multiple low energy levels. This seemingly innocent change notably enables a gap closing well below the Hermitian topological phase transition, which can be in principle simpler to achieve. Furthermore, we reveal that the energy gaps separating Majorana and trivial Andreev bound states from the quasicontinuum remain robust for the values that give rise to the zero-energy pinning effect. While reasonable values of non-Hermiticity can be indeed beneficial, very strong non-Hermitian effects can be detrimental as it might destroy superconductivity. Our findings can be therefore useful for understanding the zero-energy pinning of trivial and topological states in Majorana devices.

I. INTRODUCTION

The search of Majorana bound states (MBSs) in topological superconductors has become one of the central topics in condensed matter due to their potential for robust quantum computing [1–4]. While topological superconductivity and MBSs were initially predicted in intrinsic spin-triplet p -wave superconductors, their physical realization has been mostly pursued in superconductor-semiconductor hybrids [5–15]. In this hybrid setup, an applied magnetic field induces a topological phase transition, after which MBSs emerge as edge states with their energies oscillating around zero energy in the form of parity crossings [16–19]. In sufficiently long systems, MBSs acquire zero energy, a property that has been explored in conductance experiments but their Majorana interpretation is still puzzling [12].

One of the main issues in conductance experiments is that the reported zero bias conductance peaks (ZBCPs) are often pinned at zero energy over a range of magnetic fields [20–23], which, however, do not have a unique explanation, see also Refs. [10, 12]. In fact, ZBCPs can form due to MBSs [24–29] but also due to topologically trivial Andreev bound states (TABs) [16, 30–41], with both types of states susceptible to a zero-energy pinning effect. In the case of MBSs, it has been shown that electronic interactions [42, 43] and dissipation [44–47] are possible mechanisms for inducing a zero-energy pinning, while very strong SOC [33, 48, 49] or multiple bands [50] are needed for the zero-energy pinning of TABs. While disorder and multiple bands are intrinsic in superconductor-

semiconductor system and thus difficult to control, the fabrication of cleaner and lower dimensional samples can in principle mitigate these effects. However, the effect of dissipation, naturally appearing when attaching normal reservoirs in transport measurements [10, 12], cannot be avoided, thus highlighting its relevance on the formation of MBSs and TABs.

The effect of dissipation has also been shown to have profound consequences beyond its role as a zero-energy pinning mechanism of MBSs. Indeed, dissipation renders the system non-Hermitian and enables entirely novel topological phases that do not exist in the Hermitian realm [51, 52] as well as intriguing bulk Fermi arcs [53–58] and unusual transport properties [44, 46, 59–65]. These exotic phenomena originate from the emergence of singular points in parameter space known as *exceptional points* (EPs), defined as points where two or more eigenvalues (and their respective eigenfunctions) coalesce [66–75]. Despite the unavoidable presence of dissipation in superconductor-semiconductor systems, the impact of EPs on superconducting systems hosting simultaneously TABs and MBSs still remains an open question. Specially, superconducting systems with a homogeneous dissipation in space remain unexplored. By characterizing the role of dissipation, it would be possible to advance the understanding of Majorana devices.

In this work, we consider two one-dimensional (1D) superconducting systems with Rashba spin-orbit coupling (SOC) under a Zeeman field and study the response of their low-energy spectrum to non-Hermitian effects when coupling to ferromagnet reservoirs or leads. In particu-

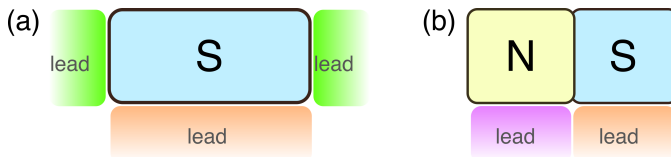


FIG. 1. Sketch of the studied non-Hermitian superconducting systems, where non-Hermiticity appears due to coupling to normal reservoirs or leads. (a) A Rashba superconductor (S in cyan) is coupled to three leads in the normal state (green and orange boxes), which can be ferromagnetic. While the green leads are only coupled to the left and right sides of S, the orange lead is coupled to the *entire* S in an homogeneous fashion. (b) A NS junction with the *entire* N and S regions coupled to ferromagnet leads (magenta and orange boxes).

lar, we explore finite length non-Hermitian systems including a superconductor and a normal-superconductor (NS) junction coupled to ferromagnet leads as in Fig. 1, permitting us to inspect MBSs and TABSs at the same footing. In general we demonstrate that non-Hermiticity induces a zero-energy pinning of MBSs and TABSs, an effect that emerges as lines of zero real energy whose ends mark the formation of exceptional points. This zero-energy pinning effect can be controlled by the interplay of non-Hermiticity and the system parameters, such as the Zeeman field and chemical potentials. By increasing non-Hermiticity, however, the evolution of the zero-energy pinning effect of TABSs exhibits a different behaviour than that of MBSs. We also discover that an homogeneous non-Hermiticity in the superconductor transforms the Hermitian topological phase transition occurring at a single point into a zero-energy line with exceptional points, which then gives rise to a gap closing at much lower Zeeman fields. Furthermore, we show that the values of non-Hermiticity causing the zero-energy pinning effect do not affect the energy gap separating TABSs and MBSs from the quasicontinuum, revealing the beneficial effect of low dissipation. Very strong non-Hermiticity, however, can induce a zero-energy pinning of the energy gaps and also of high energy levels, which can be detrimental for Majorana applications. Our results therefore demonstrate that dissipation-induced non-Hermiticity is a potential mechanism to produce zero-energy pinning of trivial and topological states in superconductor-semiconductor systems.

The remainder of this work is organized as follows. In Section II we discuss the effective non-Hermitian Hamiltonian for a superconductor with SOC coupled to ferromagnet leads. In Section III we show the impact of non-Hermiticity on the low-energy spectrum of a finite length superconductor with homogeneous pair potential, while in Section IV we address NS junctions. Finally, in Section V, we present our conclusions.

II. EFFECTIVE NON-HERMITIAN MODEL

We are interested in exploring the impact of non-Hermiticity on trivial and topological zero-energy states in superconductor-semiconductor hybrids. For this purpose we consider a 1D superconductor with Rashba SOC, which captures the main properties of superconductor-semiconductor hybrids [15], and coupled it to normal reservoirs such that the total system is open and described by an effective non-Hermitian Hamiltonian, see Fig. 1. In particular, the 1D open system can be modelled by an effective Hamiltonian given by

$$H_{\text{eff}} = H_S + \Sigma^r(\omega = 0), \quad (1)$$

where H_S is the Hermitian Hamiltonian describing the closed superconductor with SOC, while $\Sigma^r(\omega = 0)$ is the zero-frequency retarded self-energy that incorporates the non-Hermitian effects due to coupling to normal reservoirs. Even though the self-energy is in general frequency dependent, it can be approximated by its zero-frequency version $\Sigma^r(\omega = 0)$ in the wide-band limit [76], and its form will be explicitly given below. This wide-band limit has also been shown to induce interesting non-Hermitian effects in bulk setups [58, 77, 78].

We consider that the Hermitian superconductor with SOC is under the presence of a magnetic field since we are interested in obtaining MBSs [15]. Thus, the Hermitian superconductor is modelled by a spinful one-dimensional (1D) tight-binding chain given by

$$\begin{aligned} H_S = & \varepsilon \sum_{\sigma n} c_{\sigma n}^\dagger c_{\sigma n} - \sum_{\langle n, n' \rangle} t c_{\sigma n'}^\dagger c_{\sigma n} \\ & - i \sum_{\langle n, n' \rangle} t_{n'-n}^{\text{SOC}} c_{\sigma' n'}^\dagger \sigma_{\sigma' \sigma}^y c_{\sigma n} \\ & + \sum_{\sigma, \sigma' n} B c_{\sigma' n}^\dagger \sigma_{\sigma' \sigma}^x c_{\sigma n} + \sum_{\sigma n} \Delta_n c_{\sigma n}^\dagger c_{\sigma n} + \text{H.c.}, \end{aligned} \quad (2)$$

where $c_{\sigma n}$ destroys a fermionic state with spin σ at site n that runs over all the M lattice sites of the system of length $L = Ma$, with a being the lattice spacing. Moreover, here $\varepsilon = 2t - \mu$ is the onsite energy, μ is the chemical potential that determines the filling, $t = \hbar^2/(2ma^2)$ is the hopping, m is the effective mass, and $\langle n, n' \rangle$ indicates hopping between nearest neighbor sites. Moreover, $t_{\pm 1}^{\text{SOC}} = \pm \alpha_R/(2a)$ is the the SOC hopping, where α_R is the SOC strength that defines a SOC length given by $\ell_{\text{SOC}} = \hbar^2/(m\alpha_R)$, $B = g\mu_B \mathcal{B}/2$ is the Zeeman field due to an external magnetic field \mathcal{B} along the wire and perpendicular to the SOC axis, while g is the g-factor. Furthermore, Δ_n represents the space dependent proximity-induced spin-singlet s -wave pair potential from the superconductor into the semiconductor. When the pair potential is homogenous, namely, $\Delta_n = \Delta$, then the Hermitian system is a uniform superconductor. On the contrary, when finite regions have $\Delta_n = 0$ and $\Delta_n = \Delta$, we refer

to such regions as to normal (N) and superconducting (S) regions, respectively. In this case, we have a NS junction, which will be also studied here because these junctions naturally host trivial zero-energy states [33, 37].

As already mentioned above, the effect of the normal reservoirs, here referred to as normal leads, is taken into account in the form of a zero-frequency retarded self-energy, which is commonly done for studying transport [76, 79]. Motivated by the fact that distinct normal leads are usually coupled to superconductor-semiconductor systems for carrying out transport experiments [9, 10, 12, 13], here we consider three distinct ferromagnet leads as depicted in Fig. 1. Furthermore, we note that, even though the self-energy has in general real (Re) and imaginary (Im) parts, only its Im part induces non-Hermitian effects which will be studied here; its Re part renormalizes the diagonal entries of H_S . Thus, the total self-energy can be written as

$$\Sigma^r(\omega = 0) = \Sigma_L^r + \Sigma_R^r + \Sigma_X^r, \quad (3)$$

where

$$\begin{aligned} \Sigma_L^r &= -i \sum_{\sigma} \Gamma_{1\sigma} c_{\sigma 1}^{\dagger} c_{\sigma 1}, \\ \Sigma_R^r &= -i \sum_{\sigma} \Gamma_{M\sigma} c_{\sigma M}^{\dagger} c_{\sigma M}, \\ \Sigma_X^r &= -i \sum_{\sigma n} \Gamma_{n\sigma} c_{\sigma n}^{\dagger} c_{\sigma n}, \end{aligned} \quad (4)$$

model the coupling of the Hermitian system to the left, right, and middle ferromagnet leads, respectively. See Ref. [77] for details on the derivation of Eqs. (4). Here, $\Sigma_{L(R)}^r$ has finite values at the first (last) site, where $\Gamma_{\alpha\sigma}$ characterizes the coupling of the first ($\alpha = 1$) and last site ($\alpha = M$) to the leads. Similarly, Σ_X^r is the self-energy due to coupling a lead (or leads) to the entire system with $\Gamma_{\alpha\sigma}$ and $\alpha \in (1, M)$, see orange lead in Fig. 1(a) and also magenta/orange lead in Fig. 1(b). The couplings can be written as [77] $\Gamma_{\alpha\sigma} = \pi |\tau_{\alpha}|^2 \rho_{\alpha}^{\sigma}$, being τ_{α} the hopping into the lead $\alpha = L, R, X$ from the Hermitian superconductor and ρ_{α}^{σ} the surface density of states of the lead α for spin $\sigma = \uparrow, \downarrow$.

Before going further we note that both H_S and Σ^r in Eq. (2) and Eq. (3), respectively, are given in terms of creation and annihilation operators. In this regard, we can write Eq. (1) in Nambu space $(c_{n\sigma}, c_{n\sigma}^{\dagger})$, which implies that the non-Hermitian effective Hamiltonian can be treated as a matrix in real space whose dimensions are defined by the number of lattice sites. Moreover, it is worth noting that the effective Hamiltonian has particle-hole symmetry given by $H_{\text{eff}} = -\hat{C}^{-1} H_{\text{eff}}^* \hat{C}$, where $\hat{C} = \sigma_0 \tau_x C$ and C is the complex conjugation operation [44, 80–83]; this symmetry dictates that the eigenvalues of H_{eff} come in pairs as E_n and $-E_n^*$. Furthermore, given that the spectrum of the effective Hamiltonian in Eq. (2) corresponds to the poles of a retarded Green's function, the poles (and hence the eigenvalues) reside in the the lower complex energy half-plane. This, combined with

the particle-hole symmetry imposes a real spectrum that is symmetric around zero, while an imaginary part that is negative but not symmetric around zero, as we will see below.

We are interested in exploring the impact of non-Hermiticity due to normal leads modelled by Eqs. (4) on the emergence of MBSs and TABSs in H_S modelled by Eq. (2). While the formation of MBSs [15] and TABSs [33, 35, 41] appear in closes systems and do not require the presence of leads, having closed systems coupled to leads as in Fig. 1 provides an interesting scenario to explore the impact of non-Hermiticity due to the leads on MBSs and TABSs. To address these question, we consider realistic parameters, with $\alpha_R = 20 \text{ meVnm}$ and $\Delta = 0.25 \text{ meV}$, according to experimental values reported for InSb and InAs semiconductor nanowires and Nb and Al superconductors [9]. Moreover, we take the lattice spacing of $a = 10 \text{ nm}$ and analyze systems of realistic lengths. Taking these realistic parameters, we investigate the formation of MBSs and TZABSs under non-Hermiticity by using Eq. (1).

III. NON-HERMITIAN RASHBA SUPERCONDUCTOR

We start by analyzing the impact of non-Hermiticity on the formation of MBSs in the non-Hermitian superconductor modelled by Eq. (2), with an homogeneous pair potential $\Delta_n = \Delta$ and a constant self-energy all over the system that is only given by Σ_X from Eqs. (4). For obvious reasons here we denote $X=S$ in order to highlight that the lead is coupled to the entire superconductor S, as indicated by orange lead in Fig. 1(a). Since the self-energy is taken to be constant in space all over the superconductor but spin dependent, we consider that the coupling strengths are given by $\Gamma_{n\sigma} = \Gamma_{S\sigma}$, see Eqs. (4). To investigate the emergence of MBSs under non-Hermiticity, we calculate the energy spectrum of the respective effective non-Hermitian given by Eq. (2). Since the system is non-Hermitian, its spectrum becomes complex: the real part represents the physical energy of quasiparticles, while the inverse of the imaginary part determines their lifetimes $\hbar/\text{Im}(E_n)$, see Ref. [76]. When $\Gamma_{S\uparrow} = \Gamma_{S\downarrow}$, we find that all the eigenvalues acquire the same imaginary part, whose inverse gives the same lifetime for all the eigenvalues. The situation is, however, distinct when there is an asymmetry in the couplings, namely, $\Gamma_{S\uparrow} \neq \Gamma_{S\downarrow}$, which we discuss next.

In Fig. 2(a,b) we present the complex energy spectrum as a function of the Zeeman field B for $\Gamma_{S\uparrow} = 0.15 \text{ meV}$ and $\Gamma_{S\downarrow} = 0.25 \text{ meV}$, both at $\Gamma_{S\downarrow} = 0$ for a finite non-Hermitian Rashba superconductor with $L_S = 2 \mu\text{m}$. Here, the real (Re) and imaginary (Im) eigenvalues are depicted in blue and red, respectively. For completeness, the eigenvalues in the Hermitian regime, having only Re parts and developing loops around zero energy with zero-energy parity crossings, are shown in brown. The overall

Zeeman dependence of the Re part of the non-Hermitian spectrum roughly follows its Hermitian counterpart, with a symmetric profile around zero energy due to particle-hole symmetry (Sec. II), but exhibits some important changes. At very low Zeeman fields, the Re part of the spectrum is gapped and the positive (negative) eigenvalues remain degenerate for a short range of Zeeman fields, which is, however, different for distinct energy levels, see shaded red region in Fig. 2(a,b). The ends of such degenerate Re eigenvalues mark points that are accompanied by the merging of the spin split Im parts, which signals the emergence of non-Hermitian degeneracies known as exceptional points (EPs); at these EPs we have verified that the associated eigenvectors coalesce, as expected for EPs [51, 84]. Note that having split Im parts means that the associated lifetimes are distinct; their negative and non symmetric values around zero stem from particle-hole symmetry and causality discussed in Sec. II. These EPs at finite Re energies have been shown to appear in bulk Rashba semiconductors as a unique effect due to the interplay of non-Hermiticity and SOC [78] but do not depend on superconductivity.

As the Zeeman field increases, the lowest part of the Re spectrum reduces and, notably, develops a flattened gap closing feature for a range of Zeeman fields around $B = B_c$, where $B_c = \sqrt{\mu^2 + \Delta^2}$ marks the Hermitian topological phase transition (vertical green line) after which MBSs emerge [15], see yellow shaded region in Fig. 2(a,b). The closing of the Re energy gap acquiring zero energy can be estimated from the bulk Hamiltonian [58], which, at $\mu = 0$, is bounded by $B_*^\pm = \Delta \pm \gamma$, where $\gamma = (\Gamma_{S\uparrow} - \Gamma_{S\downarrow})/2$: it evident that non-Hermiticity causes a substantial lower Zeeman field B_*^- compared to the Hermitian topological phase transition at $B_c = \Delta$ when $\mu = 0$. The non-Hermitian gap closing is initially formed by the two lowest energy levels, which, after an EP transition, stick at zero Re energy for a range of B that is distinct for each level; the respective Im parts develop loops within EPs, revealing the acquisition of distinct lifetimes. The EPs occur here at zero energy between positive and negative energy levels, which is distinct to the EPs discussed in previous paragraph happening between positive energy levels with distinct spin.

The number of energy levels undergoing EP transitions at distinct B around B_c , which also feature a gap closing, can increase depending on how strong is non-Hermiticity, see Fig. 2(a,b). However, only the lowest (positive and its negative counterpart) energy level remains at zero Re energy as B increases above B after the first gap closing. Interestingly, the Hermitian parity crossings, corresponding to the oscillating energies of MBSs, become pinned at zero Re energy, see Fig. 2(a,b). The ends of the zero Re energies around the parity crossings mark the emergence of EPs, which then determine the effect we refer to as zero-energy pinning; the zero energy Re lines between EPs is more visible in the insets of Fig. 2(a,b), where the magenta short lines mark the EPs. Inside the zero Re energy lines, the Im parts form

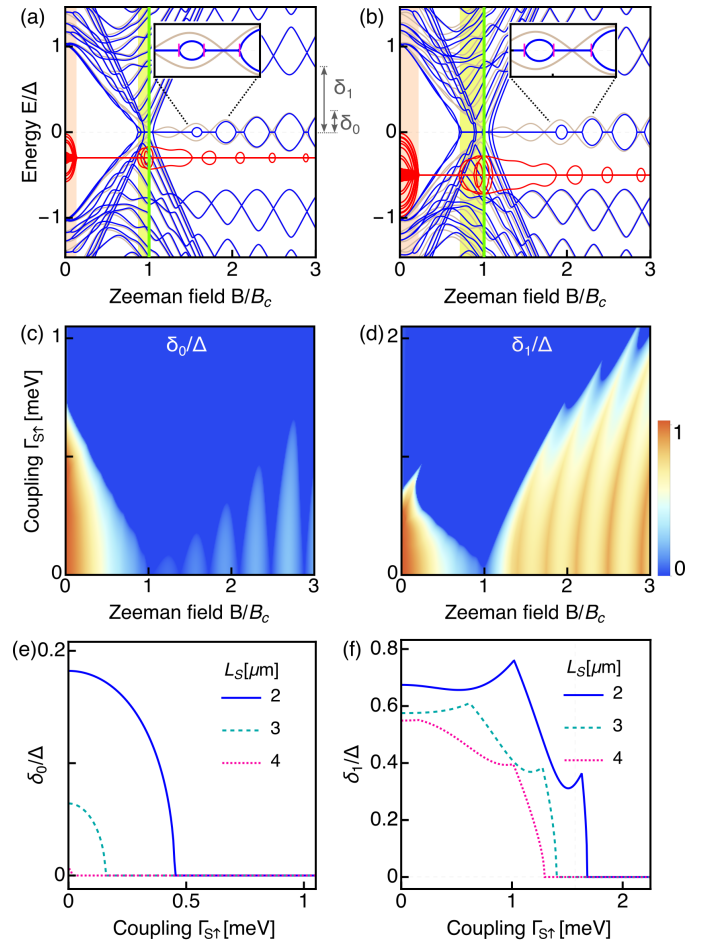


FIG. 2. (a,b) Real (blue) and imaginary (red) energy spectrum of a finite non-Hermitian Rashba superconductor as a function of the Zeeman field B at two distinct values of homogeneous non-Hermiticity $\Gamma_{S\uparrow} = 0.15\text{meV}$ and 0.25meV . Green vertical line marks the Hermitian topological phase transition at $B = B_c$, while the yellow shaded region indicates its modification due to non-Hermiticity. Brown curves in (a,b) correspond to the eigenvalues without non-Hermiticity. The insets in (a,b) show zoom-in regions of zero-energy lines between EPs (magenta marks). (c,d) Lowest and first excited real positive energies $\delta_{0,1}$ as a function of the Zeeman field B and coupling $\Gamma_{S\uparrow}$, with the blue region indicating their vanishing values; note the larger y -axis in (d) for δ_1 . (e,f) $\delta_{0,1}$ as a function of $\Gamma_{S\uparrow}$ for distinct values of the length of the superconductor L_S at $B = 2.3B_c$ of (a,b). Parameters: $\alpha_R = 20\text{meVnm}$, $\mu_S = 0.5\text{meV}$, $L_S = 2\mu\text{m}$, $\Gamma_{S\downarrow} = 0$.

loops which coalesce at the EPs: this shows that, in an open system, MBSs acquire a physical energy equal to zero and distinct imaginary parts that signal their different lifetimes. While at weak non-Hermiticity only few parity crossings exhibit the zero-energy pinning effect, large non-Hermiticity can also induce a zero-energy pinning to the zero-energy loops. It is worth noting that the parity crossings, as well as the zero-energy loops, at smaller B are more susceptible to the impact of non-Hermiticity. Thus, non-Hermiticity is able to reduce the

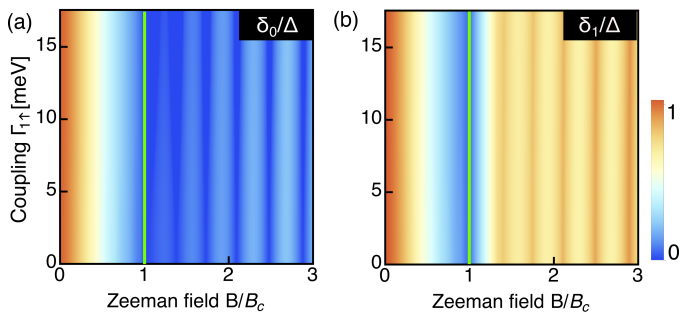


FIG. 3. (a,b) Lowest and first excited positive real energies $\delta_{0,1}$ of a non-Hermitian Rashba superconductor as a function of the Zeeman field B and non-Hermiticity only in the first site with $\Gamma_{1\uparrow} = \Gamma_{1\downarrow}$. The green vertical line marks the Hermitian topological phase transition $B = B_c$. Parameters: $\alpha_R = 20\text{meVnm}$, $\mu_S = 0.5\text{meV}$, $L_S = 2\mu\text{m}$.

value of Zeeman fields at which the gap closing occurs and also promotes a zero-energy pinning of MBSs.

To gain further insights on the role of non-Hermiticity on MBSs and the gap that protects them from the quasicontinuum, in Fig. 2(c,d) we plot the lowest and first excited Re energy levels denoted by $\delta_{0,1}$ in Fig. 2(a) as a function of the Zeeman field B and coupling $\Gamma_{S\uparrow}$. For obvious reasons, the quantities $\delta_{0,1}$ can be interpreted to be the Majorana energy and the topological gap, respectively. The blue color in Fig. 2(c,d) indicates $\delta_{0,1} = 0$, which is achieved much faster for the Majorana energy δ_0 than for the topological gap δ_1 , see that the y -axis in (b) runs over a larger values of $\Gamma_{S\uparrow}$. It is fair to say, however, that, although non-Hermiticity is indeed beneficial for inducing a zero-energy pinning of MBSs, very strong non-Hermiticity here might be detrimental as it destroys the topological gap [Fig. 2(c,d)]. The beneficial and detrimental effects of non-Hermiticity remain even when having longer systems, as shown in Fig. 2(e,f) where we plot $\delta_{0,1}$ as a function of $\Gamma_{S\uparrow}$ at $B = 2.3B_c$ for distinct L_S . Short and long systems require weak non-Hermiticity to achieve zero-energy MBSs which, interestingly, are much lower than that needed to destroy the topological gap. Therefore, non-Hermiticity due to an homogeneous coupling to ferromagnet leads can be useful to engineer zero-energy MBSs with a well-defined topological gap.

Before going further, we also discuss the impact of non-Hermiticity on the Re lowest and first excited energies $\delta_{0,1}$ when the Rashba superconductor is only coupled to a normal lead on the left (or right) side. In this situation, the effective non-Hermitian Hamiltonian contains a self-energy given by $\Sigma_{L(R)}$ in Eqs. (4), which only adds the negative imaginary contribution to the first (last) site determined by $\Gamma_{1(N)\sigma}$, unlike the case discussed above for an homogeneous non-Hermitian profile of the couplings. For simplicity, we consider that only the left side is coupled to a normal lead such that $\Gamma_{1\uparrow} = \Gamma_{1\downarrow}$ and in Fig. 3(a,b) present $\delta_{0,1}$ as a function of the Zeeman field B and coupling $\Gamma_{1\uparrow}$. Here, the blue color indicates $\delta_{0,1} = 0$. We first observe that the lowest positive energy level δ_0

does not reach zero value before B_c , even when non-Hermiticity greatly surpasses the common energy scales of the system such as pair potential and chemical potential. For $B > B_c$, we find that δ_0 , characterizing the Majorana energy, becomes zero at finite $\Gamma_{1\uparrow}$, as a result of the formation of EPs which then connect zero-energy lines around the zero-energy parity crossings, in the same fashion as found in Fig. 3(a-d). This zero-energy pinning of MBSs, however, is visible when non-Hermiticity $\Gamma_{1\sigma}$ takes very large values, see Fig. 3(a). At these large values on non-Hermiticity the first excited positive energy δ_1 only becomes zero at $B = B_c$, signaling a single point gap closing that is different to the case with homogeneous non-Hermiticity of Fig. 2 but similar to the Hermitian topological phase transition. Surprisingly, δ_1 maintains a robust finite value in the topological phase $B > B_c$, see seen in Fig. 3(b).

We have therefore shown that the effect of non-Hermiticity can be beneficial for stabilizing MBSs without destroying the topological gap. Moreover, depending on the non-Hermitian profile, it is possible to induce a topological phase transition at much lower Zeeman fields, which could be useful for mitigating the detrimental effects of magnetism on superconductivity in Majorana devices.

IV. NON-HERMITIAN RASHBA NORMAL-SUPERCONDUCTOR JUNCTION

Having discussed the impact of non-Hermiticity on MBSs emerging in a finite length Rashba superconductor, here we study how non-Hermiticity affects the low-energy spectrum of normal-superconductor (NS) junctions with Rashba SOC. NS junctions in Majorana devices are particularly relevant because they host trivial Andreev bound states (TABSS) well below the topological phase transition at $B = B_c$ by depleting the N region, see Ref. [33, 37]. The non-Hermitian NS junction is modelled by Eq. (2) but with $\Delta_n = 0$ in N and $\Delta_n = \Delta$ in S, which gives N(S) regions of distinct lengths $L_{N(S)}$. We consider two independent cases of non-Hermiticity due to homogeneously coupling the entire N or S region to a ferromagnet lead; the self-energy due to coupling to the lead is characterized by $\Gamma_{N(S)\sigma}$. The Re low-energy spectrum as a function of the Zeeman field B is presented in Fig. 4(a,b) and Fig. 4(c,d) for two values of non-Hermiticity in N and S, respectively. The Im part of the spectrum is not shown because it makes more difficult to analyze the already dense panels. For completeness we also show the Hermitian low-energy spectrum (brown curves), which exhibits parity crossings with zero-energy loops well below B_c (green vertical line) and indicated by the shaded yellow region in Fig. 4(a-d). In Fig. 4(e,f) we show the lowest and first excited energy positive Re levels $\delta_{0(1)}$ as a function of B and $\Gamma_{N\uparrow}$, where the blue color indicates $\delta_{0,1} = 0$.

The first observation is that in the two situations, with

non-Hermiticity in N or S, a zero-energy pinning of both TABSs and MBSs occurs, with similarities but also with some slight differences, see Fig. 4(a-d) and also Fig. 4(e,f). Among the similarities is that the zero-energy pinning occurs between EP transitions: the ends of the zero-energy lines mark the formation of EPs. We have verified that the Im parts form loops between EPs as those seen in Fig. 2(a,b), while they and the associated wavefunctions coalesce at EPs as expected at EPs. Another similarity is that increasing the strength of non-Hermiticity favors the appearance of longer zero-energy lines between EPs, which corresponds to a zero-energy pinning effect for a larger range of Zeeman fields, as seen by comparing Fig. 4(a) and Fig. 4(b) or Fig. 4(c) and Fig. 4(d).

Among the differences between non-Hermiticity in N and S, we find distinct impact of non-Hermiticity on the lowest energy levels and also on the excited energies. For instance the zero-energy crossings in the trivial phase ($B < B_c$) and topological phase ($B > B_c$) are more susceptible to non-Hermiticity in S than in N. This is seen in Fig. 4(a,c) by noting that even a smaller value of non-Hermiticity in S produces a stronger zero-energy pinning in the trivial phase, see Fig. 4(c). The different response remains even when the strength of non-Hermiticity in N and S are the same, as seen the larger zero-energy lines in Fig. 4(d) as compared to Fig. 4(b). Of course that stronger values of non-Hermiticity in N have the potential to produce larger regions with zero-energy pinning but then MBSs acquire zero energy faster than TABSs, see Fig. 4(e). Another difference is that the excited spectrum remains largely unaffected for reasonable values of non-Hermiticity in N while the same is not true when non-Hermiticity is in S, see e.g., Fig. 4(a,c). As a result, having non-Hermiticity in N leads to a gap closing feature occurring at a single point at $B = B_c$ and not accompanied by additional states [Fig. 4(a,b)]. In contrast, for non-Hermiticity in S, the gap closing can occur at a continuous set of points as a flattened zero-energy line whose ends mark the formation of EPs [Fig. 4(d)]; this is similar to what we saw in Fig. 2(a,b) for the gap closing. It is also important to say that stronger non-Hermiticity in N can also affect δ_1 , inducing it to even vanish either for $B < B_c$ or $B > B_c$, as seen in Fig. 4(f). In this case, however, in the topological phase δ_1 vanishes but at stronger non-Hermiticity values than in the trivial phase. Despite the differences, it is clear that non-Hermiticity induces a zero-energy pinning in both MBSs and TABSs.

To gain further understanding on the impact of non-Hermiticity on the TABSs and MBSs, in Fig. 5(a,b) we plot the Re low-energy spectrum as a function of the chemical potential in N μ_N at $B < B_c$ and $B > B_c$. In Fig. 5(c,d) we plot the lowest Re positive energy δ_0 as a function of the chemical potential μ_N and the coupling $\Gamma_{N\uparrow}$, while in Fig. 5(e,f) we do the same for the first excited positive Re energy level δ_1 . As we have done before, in brown color we also show the Hermitian energy levels, which form loops around zero-energy with parity crossings. These oscillatory zero-energy loops reflect the

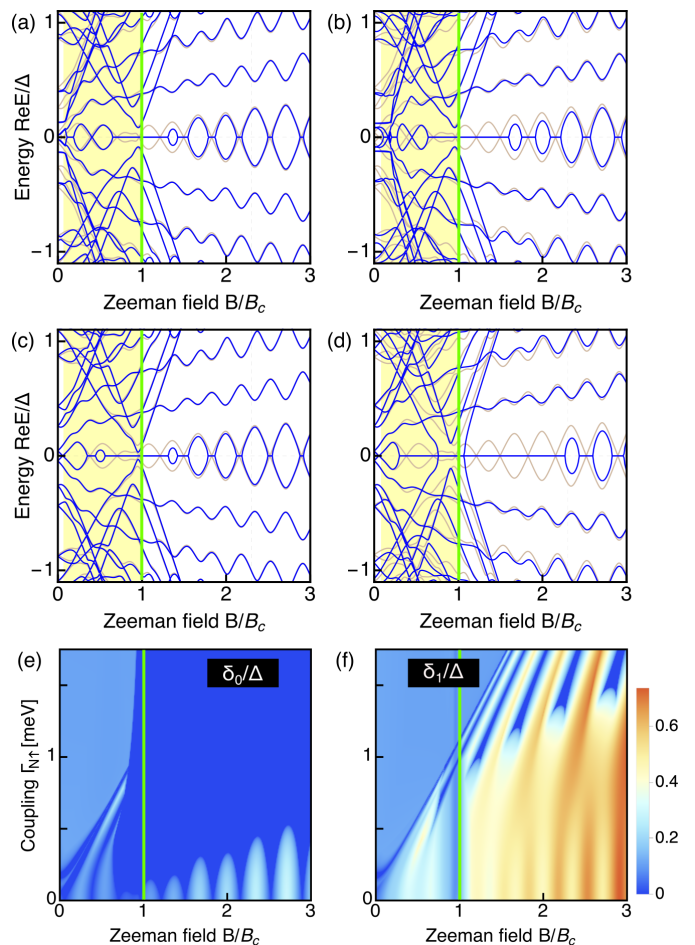


FIG. 4. (a,b) Real low energy spectrum as a function of the Zeeman field for a finite NS Rashba junction with a homogeneous non-Hermiticity in N characterized by $\Gamma_{N\uparrow} = 0.15\text{meV}$ (a) and $\Gamma_{N\uparrow} = 0.25\text{meV}$ (b). (c,d) The same as in (a,b) but with a homogeneous non-Hermiticity in S characterized by $\Gamma_{S\uparrow} = 0.1\text{meV}$ (c) and $\Gamma_{S\uparrow} = 0.25\text{meV}$ (d). The brown curves in (a-d) correspond to the eigenvalues in the Hermitian regime, showing trivial ABSs below the Hermitian topological phase transition at $B = B_c$. The green vertical line in (a-f) marks $B = B_c$, while the shaded yellow regions indicate the Zeeman fields at which trivial ABSs form. (e,f) Lowest and first excited real positive energies $\delta_{0,1}$ as a function of $\Gamma_{N\uparrow}$ and B . Parameters: $\alpha_R = 20\text{meVnm}$, $\mu_N = 0.05\text{meV}$, $\mu_S = 0.5\text{meV}$, $L_S = 1\mu\text{m}$, $L_N = 1\mu\text{m}$, $\Gamma_{N\downarrow} = 0$, $\Gamma_{S\downarrow} = 0$.

formation of MBSs and TABSs in the topological and trivial phases, respectively, see Ref. [33]. The first feature we observe is that the parity crossings transform into zero-energy lines with their ends marking EPs, reflecting that the zero-energy pinning of MBSs and TABSs can be controlled by μ_N , see Fig. 5(a,b). Although the zero-energy pinning effect is similar in the trivial and topological phases, the impact of non-Hermiticity on the parity crossings in the topological phase are more likely to give rise to larger zero-energy lines [Fig. 5(a,b)]. In fact, by increasing non-Hermiticity via $\Gamma_{N\uparrow}$, the trivial parity crossings exhibit a zero-energy pinning but not

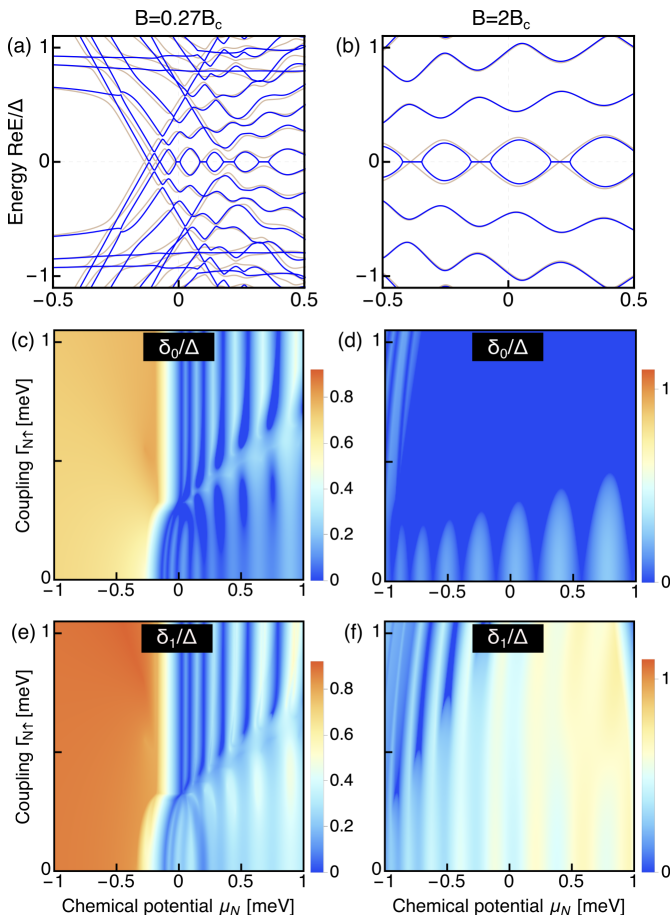


FIG. 5. (a,b) Real low-energy spectrum for a finite NS Rashba junction as a function of the chemical potential in N μ_N at B in the trivial (a) and topological (b) regimes. Here, non-Hermiticity is finite and homogeneous in N and characterized by $\Gamma_{N\uparrow} = 0.15\text{meV}$. (c,d) Lowest positive real energy δ_0 as a function of μ_N and $\Gamma_{N\uparrow}$. (e,f) The same as in (c,d) but for the first excited positive real energy δ_1 . Parameters: $\alpha_R = 20\text{meVnm}$, $\mu_S = 0.5\text{meV}$, $L_S = 1\mu\text{m}$, $L_N = 1\mu\text{m}$, $\Gamma_{N\downarrow} = 0$.

all of them form zero-energy lines at the same value of non-Hermiticity [Fig. 5(c)]. This is in contrast to what occurs for the parity crossings in the topological phase, where all of them simultaneously feel the impact of non-Hermiticity and exhibit a zero-energy pinning [Fig. 5(d)]. Furthermore, the energy gap separating the TABSs and MBSs from the quasicontinuum (δ_1) is approximately robust for small values of $\Gamma_{N\uparrow}$, but can undergo EP transitions at zero energy when such $\Gamma_{N\uparrow}$ is rather strong, as seen in Fig. 5(e,f).

Non-Hermiticity is, therefore, able to stabilize both MBSs and TABSs at zero-energy, a zero-energy pinning effect that can be controlled by the Zeeman field or chemical potential of the normal region [85]. While zero-energy pinning can be beneficial, it could also bring difficulties because it will be more challenging to identify the origin of such stable zero-energy states. Moreover, even though reasonable values of non-Hermiticity do not

considerably affect the energy gap separating MBSs or TABSs from the quasicontinuum, strong non-Hermiticity can be detrimental.

V. CONCLUSIONS

In conclusion, we have investigated the impact of non-Hermiticity on the low-energy spectrum of finite superconducting systems with Rashba spin-orbit coupling, where non-Hermitian effects arise due to coupling to normal or ferromagnet leads. We have demonstrated that non-Hermiticity transforms the Hermitian parity crossings of the oscillatory Majorana energies into lines of zero real energy whose ends mark the formation of exceptional points. We have also found that non-Hermiticity induces a similar zero-energy pinning effect of trivial Andreev bound states, which appear well below the topological phase transition in the Hermitian regime. However, we obtained that Majorana bound states can be more susceptible to non-Hermiticity than trivial Andreev bound states, specially when non-Hermiticity is present all over the superconductor or normal-superconductor junctions. Moreover, we have shown that the values of non-Hermiticity inducing the zero-energy pinning effect do not damage the energy gap that separates the Majorana or Andreev bound states from the quasicontinuum, thus highlighting the beneficial effect of non-Hermiticity. We found that the zero-energy pinning effect can be highly controllable by the interplay of non-Hermiticity and the system parameters, such as Zeeman field and chemical potentials.

We have also revealed that non-Hermiticity has an important effect on the Hermitian topological phase transition when its profile is homogeneous all over the superconductor. In this case we have discovered that the energy gap undergoes a zero-energy pinning effect due to exceptional points, leading to a flattened gap closing feature unlike the single point Hermitian topological phase transition. This effect suggests that it is possible to achieve a topological phase transition at Zeeman fields much lower than in the Hermitian regime, which is important because strong Zeeman fields are often seen as detrimental for superconductivity. However, good control over the non-Hermitian mechanism is needed because very strong non-Hermiticity not only has the potential to induce large zero-energy pinning ranges but it can also destroy the energy gap. Given that Majorana devices are often coupled to normal leads, where non-Hermitian effects are intrinsic, our results can be helpful for understanding the possible mechanisms giving rise to zero-energy states.

VI. ACKNOWLEDGEMENTS

We thank R. Aguado, M. Sato and Y. Tanaka for insightful discussions. We acknowledge financial support

from the Swedish Research Council (Vetenskapsrådet Grant No. 2021-04121) and the Carl Trygger's Foundation (Grant No. 22: 2093). The computations were enabled by resources provided by the National

Academic Infrastructure for Supercomputing in Sweden (NAISS), partially funded by the Swedish Research Council through grant agreement no. 2022-06725.

-
- [1] S. D. Sarma, M. Freedman, and C. Nayak, Majorana zero modes and topological quantum computation, *npj Quantum Inf.* **1**, 15001 (2015).
- [2] C. Beenakker, Search for non-Abelian Majorana braiding statistics in superconductors, *SciPost Phys. Lect. Notes* , 15 (2020).
- [3] R. Aguado and L. P. Kouwenhoven, Majorana qubits for topological quantum computing, *Phys. Today* **73**, 44 (2020).
- [4] R. Aguado, A perspective on semiconductor-based superconducting qubits, *Appl. Phys. Lett.* **117** (2020).
- [5] Y. Tanaka, M. Sato, and N. Nagaosa, Symmetry and topology in superconductors—odd-frequency pairing and edge states—, *J. Phys. Soc. Jpn.* **81**, 011013 (2011).
- [6] M. Sato and S. Fujimoto, Majorana fermions and topology in superconductors, *J. Phys. Soc. Jpn.* **85**, 072001 (2016).
- [7] M. Sato and Y. Ando, Topological superconductors: a review, *Rep. Prog. Phys.* **80**, 076501 (2017).
- [8] R. Aguado, Majorana quasiparticles in condensed matter, *Riv. Nuovo Cimento* **40**, 523 (2017).
- [9] R. M. Lutchyn, E. P. Bakkers, L. P. Kouwenhoven, P. Krogstrup, C. M. Marcus, and Y. Oreg, Majorana zero modes in superconductor–semiconductor heterostructures, *Nat. Rev. Mater.* **3**, 52 (2018).
- [10] H. Zhang, D. E. Liu, M. Wimmer, and L. P. Kouwenhoven, Next steps of quantum transport in Majorana nanowire devices, *Nat. Commun.* **10**, 5128 (2019).
- [11] S. M. Frolov, M. J. Manfra, and J. D. Sau, Topological superconductivity in hybrid devices, *Nat. Phys.* **16**, 718 (2020).
- [12] E. Prada, P. San-Jose, M. W. de Moor, A. Geresdi, E. J. Lee, J. Klinovaja, D. Loss, J. Nygård, R. Aguado, and L. P. Kouwenhoven, From Andreev to Majorana bound states in hybrid superconductor–semiconductor nanowires, *Nat. Rev. Phys.* **2**, 575 (2020).
- [13] K. Flensberg, F. von Oppen, and A. Stern, Engineered platforms for topological superconductivity and Majorana zero modes, *Nat. Rev. Mater.* **6**, 944 (2021).
- [14] P. Marra, Majorana nanowires for topological quantum computation, *J. Appl. Phys.* **132**, 231101 (2022).
- [15] Y. Tanaka, S. Tamura, and J. Cayao, Theory of Majorana zero modes in unconventional superconductors, *Prog. Theor. Exp. Phys.* , ptae065 (2024).
- [16] E. Prada, P. San-Jose, and R. Aguado, Transport spectroscopy of *ns* nanowire junctions with Majorana fermions, *Phys. Rev. B* **86**, 180503 (2012).
- [17] S. Das Sarma, J. D. Sau, and T. D. Stanescu, Splitting of the zero-bias conductance peak as smoking gun evidence for the existence of the Majorana mode in a superconductor-semiconductor nanowire, *Phys. Rev. B* **86**, 220506 (2012).
- [18] D. Rainis, L. Trifunovic, J. Klinovaja, and D. Loss, Towards a realistic transport modeling in a superconducting nanowire with Majorana fermions, *Phys. Rev. B* **87**, 024515 (2013).
- [19] J. Cayao, P. San-Jose, A. M. Black-Schaffer, R. Aguado, and E. Prada, Majorana splitting from critical currents in Josephson junctions, *Phys. Rev. B* **96**, 205425 (2017).
- [20] S. M. Albrecht, A. P. Higginbotham, M. Madsen, F. Kuemmeth, T. S. Jespersen, J. Nygård, P. Krogstrup, and C. M. Marcus, Exponential protection of zero modes in Majorana islands, *Nature* **531**, 206 (2016).
- [21] J. Chen, B. D. Woods, P. Yu, M. Hocevar, D. Car, S. R. Plissard, E. P. A. M. Bakkers, T. D. Stanescu, and S. M. Frolov, Ubiquitous non-Majorana zero-bias conductance peaks in nanowire devices, *Phys. Rev. Lett.* **123**, 107703 (2019).
- [22] H. Zhang, M. W. A. de Moor, J. D. S. Bommer, D. Xu, G. Wang, N. van Loo, C.-X. Liu, S. Gazibegovic, J. A. Logan, D. Car, R. L. M. O. het Veld, P. J. van Veldhoven, S. Koelling, M. A. Verheijen, M. Pendharkar, D. J. Pennachio, B. Shojaei, J. S. Lee, C. J. Palmstrom, E. P. A. M. Bakkers, S. D. Sarma, and L. P. Kouwenhoven, Large zero-bias peaks in InSb-Al hybrid semiconductor-superconductor nanowire devices, *arXiv: 2101.11456* (2021).
- [23] M. Valentini, F. Peñaranda, A. Hofmann, M. Brauns, R. Hauschild, P. Krogstrup, P. San-Jose, E. Prada, R. Aguado, and G. Katsaros, Nontopological zero-bias peaks in full-shell nanowires induced by flux-tunable Andreev states, *Science* **373**, 82 (2021).
- [24] Y. Tanaka and S. Kashiwaya, Theory of tunneling spectroscopy of *d*-wave superconductors, *Phys. Rev. Lett.* **74**, 3451 (1995).
- [25] S. Kashiwaya, Y. Tanaka, M. Koyanagi, and K. Kajimura, Theory for tunneling spectroscopy of anisotropic superconductors, *Phys. Rev. B* **53**, 2667 (1996).
- [26] S. Kashiwaya and Y. Tanaka, Tunneling effects on surface bound states in unconventional superconductors, *Rep. Prog. Phys.* **63**, 1641 (2000).
- [27] C. J. Bolech and E. Demler, Observing Majorana bound states in *p*-wave superconductors using noise measurements in tunneling experiments, *Phys. Rev. Lett.* **98**, 237002 (2007).
- [28] K. T. Law, P. A. Lee, and T. K. Ng, Majorana fermion induced resonant Andreev reflection, *Phys. Rev. Lett.* **103**, 237001 (2009).
- [29] K. Flensberg, Tunneling characteristics of a chain of Majorana bound states, *Phys. Rev. B* **82**, 180516 (2010).
- [30] D. Bagrets and A. Altland, Class *D* spectral peak in Majorana quantum wires, *Phys. Rev. Lett.* **109**, 227005 (2012).
- [31] D. I. Pikulin, J. P. Dahlhaus, M. Wimmer, H. Schomerus, and C. W. J. Beenakker, A zero-voltage conductance peak from weak antilocalization in a Majorana nanowire, *New J. Phys.* **14**, 125011 (2012).
- [32] G. Kells, D. Meidan, and P. W. Brouwer, Near-zero-energy end states in topologically trivial spin-orbit coupled superconducting nanowires with a smooth confine-

- ment, Phys. Rev. B **86**, 100503 (2012).
- [33] J. Cayao, E. Prada, P. San-Jose, and R. Aguado, Sns junctions in nanowires with spin-orbit coupling: Role of confinement and helicity on the subgap spectrum, Phys. Rev. B **91**, 024514 (2015).
- [34] C. Reeg, O. Dmytruk, D. Chevallier, D. Loss, and J. Klinovaja, Zero-energy Andreev bound states from quantum dots in proximitized rashba nanowires, Phys. Rev. B **98**, 245407 (2018).
- [35] O. A. Awoga, J. Cayao, and A. M. Black-Schaffer, Supercurrent detection of topologically trivial zero-energy states in nanowire junctions, Phys. Rev. Lett. **123**, 117001 (2019).
- [36] S. Das Sarma and H. Pan, Disorder-induced zero-bias peaks in Majorana nanowires, Phys. Rev. B **103**, 195158 (2021).
- [37] J. Cayao and A. M. Black-Schaffer, Distinguishing trivial and topological zero-energy states in long nanowire junctions, Phys. Rev. B **104**, L020501 (2021).
- [38] J. Cayao and P. Burset, Confinement-induced zero-bias peaks in conventional superconductor hybrids, Phys. Rev. B **104**, 134507 (2021).
- [39] B. S. de Mendonça, A. L. R. Manesco, N. Sandler, and L. G. G. V. Dias da Silva, Near zero energy caroli-de gennes-matricon vertex states in the presence of impurities, Phys. Rev. B **107**, 184509 (2023).
- [40] L. Baldo, L. G. D. Da Silva, A. M. Black-Schaffer, and J. Cayao, Zero-frequency supercurrent susceptibility signatures of trivial and topological zero-energy states in nanowire junctions, Supercond. Sci. Technol. **36**, 034003 (2023).
- [41] O. A. Awoga, M. Leijnse, A. M. Black-Schaffer, and J. Cayao, Mitigating disorder-induced zero-energy states in weakly coupled superconductor-semiconductor hybrid systems, Phys. Rev. B **107**, 184519 (2023).
- [42] F. Domínguez, J. Cayao, P. San-Jose, R. Aguado, A. L. Yeyati, and E. Prada, Zero-energy pinning from interactions in Majorana nanowires, npj Quantum Mater. **2**, 13 (2017).
- [43] S. D. Escribano, A. L. Yeyati, and E. Prada, Interaction-induced zero-energy pinning and quantum dot formation in Majorana nanowires, Beilstein J. Nanotechnol. **9**, 2171 (2018).
- [44] P. San-José, J. Cayao, E. Prada, and R. Aguado, Majorana bound states from exceptional points in non-topological superconductors, Sci. Rep. **6**, 21427 (2016).
- [45] J. Avila, F. Peñaranda, E. Prada, P. San-Jose, and R. Aguado, Non-Hermitian topology as a unifying framework for the Andreev versus Majorana states controversy, Commun. Phys. **2**, 133 (2019).
- [46] J. Cayao and M. Sato, Non-Hermitian phase-biased Josephson junctions, arXiv:2307.15472 (2023).
- [47] A. K. Ghosh and A. M. Black-Schaffer, Majorana zero-modes in a dissipative Rashba nanowire, arXiv:2403.00419 (2024).
- [48] R. V. Mishmash, D. Aasen, A. P. Higginbotham, and J. Alicea, Approaching a topological phase transition in Majorana nanowires, Phys. Rev. B **93**, 245404 (2016).
- [49] O. Dmytruk, D. Loss, and J. Klinovaja, Pinning of Andreev bound states to zero energy in two-dimensional superconductor-semiconductor rashba heterostructures, Phys. Rev. B **102**, 245431 (2020).
- [50] B. D. Woods, J. Chen, S. M. Frolov, and T. D. Stanescu, Zero-energy pinning of topologically trivial bound states in multiband semiconductor-superconductor nanowires, Phys. Rev. B **100**, 125407 (2019).
- [51] Y. Ashida, Z. Gong, and M. Ueda, Non-Hermitian physics, Adv. Phys. **69**, 249 (2020).
- [52] N. Okuma and M. Sato, Non-Hermitian topological phenomena: a review, Annu. Rev. Condens. Matter Phys. **14**, 83 (2023).
- [53] V. Kozii and L. Fu, Non-Hermitian topological theory of finite-lifetime quasiparticles: Prediction of bulk Fermi arc due to exceptional point, arXiv:1708.05841 (2017).
- [54] A. A. Zyuzin and A. Y. Zyuzin, Flat band in disorder-driven non-Hermitian weyl semimetals, Phys. Rev. B **97**, 041203 (2018).
- [55] H. Zhou, C. Peng, Y. Yoon, C. W. Hsu, K. A. Nelson, L. Fu, J. D. Joannopoulos, M. Soljačić, and B. Zhen, Observation of bulk Fermi arc and polarization half charge from paired exceptional points, Science **359**, 1009 (2018).
- [56] T. Yoshida, R. Peters, and N. Kawakami, Non-Hermitian perspective of the band structure in heavy-fermion systems, Phys. Rev. B **98**, 035141 (2018).
- [57] T. Bessho, K. Kawabata, and M. Sato, Topological classification of non-Hermitian gapless phases: Exceptional points and bulk fermi arcs, in *Proc. Int. Conf. on Strongly Correlated Electron Systems (SCES2019)* (Physical Society of Japan, 2019) Chap. 30, p. 011098.
- [58] J. Cayao and A. M. Black-Schaffer, Bulk Bogoliubov Fermi arcs in non-Hermitian superconducting systems, Phys. Rev. B **107**, 104515 (2023).
- [59] T. M. Philip, M. R. Hirsbrunner, and M. J. Gilbert, Loss of Hall conductivity quantization in a non-Hermitian quantum anomalous Hall insulator, Phys. Rev. B **98**, 155430 (2018).
- [60] M. Lu, X.-Z. Liu, H. Li, Z.-Q. Zhang, J. Liu, and X. C. Xie, Dissipation-enhanced unidirectional transport in topological systems, Phys. Rev. B **109**, 165402 (2024).
- [61] C.-A. Li, H.-P. Sun, and B. Trauzettel, Anomalous Andreev bound states in non-Hermitian Josephson junctions, arXiv:2307.04789 (2023).
- [62] R.-P. Riwar, Fractional charges in conventional sequential electron tunneling, Phys. Rev. B **100**, 245416 (2019).
- [63] M. A. Javed, J. Schwibbert, and R.-P. Riwar, Fractional Josephson effect versus fractional charge in superconducting-normal metal hybrid circuits, Phys. Rev. B **107**, 035408 (2023).
- [64] R. Mélin, Multiterminal ballistic Josephson junctions coupled to normal leads, Phys. Rev. B **105**, 155418 (2022).
- [65] J. Cayao and R. Aguado, Non-hermitian minimal kitaev chains, arXiv: 2406.18974 (2024).
- [66] T. Kato, *Perturbation theory of linear operators* (Springer, New York, 1966).
- [67] W. Heiss, Exceptional points—their universal occurrence and their physical significance, Czechoslov. J. Phys. **54**, 1091 (2004).
- [68] M. V. Berry, Physics of nonhermitian degeneracies, Czechoslov. J. Phys. **54**, 1039 (2004).
- [69] W. D. Heiss, The physics of exceptional points, J. Phys. A Math. Theor. **45**, 444016 (2012).
- [70] C. Dembowski, H.-D. Gräf, H. L. Harney, A. Heine, W. D. Heiss, H. Rehfeld, and A. Richter, Experimental observation of the topological structure of exceptional points, Phys. Rev. Lett. **86**, 787 (2001).
- [71] S.-B. Lee, J. Yang, S. Moon, S.-Y. Lee, J.-B. Shim, S. W. Kim, J.-H. Lee, and K. An, Observation of an exceptional

- point in a chaotic optical microcavity, *Phys. Rev. Lett.* **103**, 134101 (2009).
- [72] Y. Choi, S. Kang, S. Lim, W. Kim, J.-R. Kim, J.-H. Lee, and K. An, Quasieigenstate coalescence in an atom-cavity quantum composite, *Phys. Rev. Lett.* **104**, 153601 (2010).
- [73] T. Gao, E. Estrecho, K. Bliokh, T. Liew, M. Fraser, S. Brodbeck, M. Kamp, C. Schneider, S. Höfling, Y. Yamamoto, *et al.*, Observation of non-Hermitian degeneracies in a chaotic exciton-polariton billiard, *Nature* **526**, 554 (2015).
- [74] J. Doppler, A. A. Mailybaev, J. Böhm, U. Kuhl, A. Girschik, F. Libisch, T. J. Milburn, P. Rabl, N. Moiseyev, and S. Rotter, Dynamically encircling an exceptional point for asymmetric mode switching, *Nature* **537**, 76 (2016).
- [75] T. Yoshida, R. Peters, N. Kawakami, and Y. Hatsugai, Symmetry-protected exceptional rings in two-dimensional correlated systems with chiral symmetry, *Phys. Rev. B* **99**, 121101 (2019).
- [76] S. Datta, *Electronic transport in mesoscopic systems* (Cambridge university press, 1997).
- [77] J. Cayao and A. M. Black-Schaffer, Exceptional odd-frequency pairing in non-Hermitian superconducting systems, *Phys. Rev. B* **105**, 094502 (2022).
- [78] J. Cayao, Exceptional degeneracies in non-Hermitian Rashba semiconductors, *J. Condens. Matter Phys.* **35**, 254002 (2023).
- [79] J. C. Cuevas, A. Martín-Rodero, and A. L. Yeyati, Hamiltonian approach to the transport properties of superconducting quantum point contacts, *Phys. Rev. B* **54**, 7366 (1996).
- [80] D. I. Pikulin and Y. V. Nazarov, Topological properties of superconducting junctions, *JETP Lett.* **94**, 693 (2012).
- [81] D. I. Pikulin and Y. V. Nazarov, Two types of topological transitions in finite Majorana wires, *Phys. Rev. B* **87**, 235421 (2013).
- [82] P. Ioselevich and M. Feigel'man, Tunneling conductance due to a discrete spectrum of Andreev states, *New J. Phys.* **15**, 055011 (2013).
- [83] C. W. J. Beenakker, Random-matrix theory of majorana fermions and topological superconductors, *Rev. Mod. Phys.* **87**, 1037 (2015).
- [84] E. J. Bergholtz, J. C. Budich, and F. K. Kunst, Exceptional topology of non-Hermitian systems, *Rev. Mod. Phys.* **93**, 015005 (2021).
- [85] Non-Hermiticity, however, cannot help distinguishing between zero-energy TABSs and zero-energy MBSs. Nevertheless, the distinct features of the spectrum in the trivial (with TABSs) and topological (with MBSs) phases presented in Figs. 4 and 5 shows that being able to control the amount of non-Hermiticity can be useful to distinguish between TABSs and MBSs. However, this task is challenging because it involves to have good control over the coupling to reservoirs.